This is the Author Accepted Manuscript (postprint) of:
Tacchini et al., 2011, J Mater Sci. 46:2097–2104
https://doi.org/10.1007/s10853-010-5044-9

Anatase nanotubes synthesized by a template method and their application as a green photocatalyst

I. Tacchini, E. Terrado*, A. Ansón, M. T. Martínez
*Corresponding author: E. Terrado (eterrado@icb.csic.es)
Instituto de Carboquímica, CSIC, Zaragoza, Spain

Abstract

Anatase nanotubes were synthesized by a template method from four different titanium precursors. Anodized aluminum oxide membranes with a 200-nm pore diameter were used as templates. The resulting nanostructures were characterized by electron micros- copies, Raman spectroscopy, X-ray diffraction and nitro- gen adsorption. Their photoactivities towards methylene blue dye decomposition were measured and compared with commercial anatase powder (Aldrich, [99%, -325 mesh). Anatase nanotubes obtained from Ti isopropoxide exhibited the longest hollow tubular structures with less amorphous material and the highest surface area, 56 m^2 g^{-1}. Despite TiO2 nanotubes showing lower photocatalytic activity than commercial anatase, the possibility of their recovery through several cycles and the feasibility of their utilization in continuous cycling processing make them potential materials of interest in green chemistry

Keywords: TiO2 nanotubes; anatase; photocatalysis; template synthesis; green chemistry

Introduction

The photoinduced mechanism [1] that takes place in titanium oxide (TiO2) has been studied since the end of the 1960s. This process has been given a wide range of applications in several fields such as photovoltaics [2, 3], environmental photocatalysis [4], and most recently, in the area of superhydrophilicity [5, 6]. Even though all photo-induced phenomena imply surface bound redox reactions, it is important to note that the type of photochemistry involved in photocatalysis reactions and hydrophilicity phenomena are completely different and can occur simultaneously on the same surface [7].

Absorption of a photon with sufficient energy by a TiO2 crystal leads to a charge separation owing to an electron promotion to the conduction band and a resulting hole in the valence band [8]. The electron–hole pair tends to migrate to the crystal surface. If the pair reaches the surface without recombination, then use can be made of the hole or the electron (depending on the final application), e.g. for electrical current generation in photovoltaic solar cells, for hydrogen production or for antifogging surfaces [2–6]. Another interesting application for TiO2 has been found in the field of self-cleaning surfaces and contaminant destruction. One example of these undesirable substances is dye. Large amounts of dyes are produced by industry every year, and their uncontrolled discharge into bodies of water can cause drastic damage to the aquatic environment [9]. Dyes are environmentally harmful even at low concentrations because of the induced change in the color of water. This effect is deeply unpleasant because it limits the access to sunlight by aquatic flora, reducing the photo- synthetic action within the ecosystem [10]. Dye elimination is complicated by conventional wastewater treatments owing to its inherent high values of chemical oxygen demand (COD) and biochemical oxygen demand (BOD). In this context, heterogeneous photocatalysis may be used as an alternative solution for dye degradation, and TiO2 could be a considerable candidate because of its high catalytic efficiency, high chemical stability, low cost and non- toxic nature. However, TiO2 suspensions in water show high stability, which hinders separation of the catalyst from water and, consequently, its recovery and reuse [11]. A viable solution to this drawback could be found in developing new TiO2-based morphologies in nanostructured materials.

Anatase and rutile are the photosensitive crystalline phases of TiO2. The required energy for the electron pro- motion from the valence band to the conduction band is 3.2 eV for anatase and 3.0 eV for rutile [12, 13]. One of the most popular strategies to ensure the success of the photoinduced mechanisms in TiO2 materials is by reducing the migration path to the crystal surface (and consequently the possibility of the hole–electron pair recombination) whilst obtaining a larger catalytic surface. Hence, many efforts have been made in the last years to produce TiO2 nanostructured materials shaped like small particles [14, 15], tubes [16, 17] and rods [18, 19] with nanometric diameters. In particular, TiO2 nanotubes can be synthesized in different ways: the hydrothermal method [20, 21], the template method [22, 23], and the electrochemical method [24] including electrochemical oxidation of Ti metal in electrolytes containing fluoride ions [25, 26]. In this study, we obtained anatase nanotubes using a template-based methodology inspired by the impregnation–decomposition method reported by Michailowski et al. [27]. In addition to titanium isopropoxide precursor reported in [27], three more precursors and a simpler set up were used. This approach is based on a template containing tubular channels with nanometric diameters. The channels are filled with different titanium sources. After an appropriate thermal treatment and template removal, the obtained material consists of TiO2 nanotubes with the same dimensional features as the template channels. We chose anodized aluminum oxide membranes as the nanotubes templates. These membranes were commercially available with a well-defined channel diameter size. The material characterization by electron microscopies, X-ray diffraction (XRD), nitrogen adsorption and Raman techniques allowed us to determine the best titanium source and the optimized experimental conditions for obtaining anatase nanotubes with the highest specific catalytic surface. Finally, we tested the ability of our materials to destroy a model compound, methylene blue (MB), and evaluated the efficiency of its recovery in comparison with commercial anatase (Aldrich, [99%, -325 mesh).

Experimental methods

TiO2 nanotube production and characterization

Experiments were carried out using porous alumina membranes (Whatman Anodisc) as templates. These membranes are made of high-purity anodized alumina and exhibit high

pore densities and narrow pore size distributions with an average diameter of 200 nm (Fig. 1). Each titanium precursor (TiP) was poured into a schlenk (Fig. 2) and immersed in liquid nitrogen to freeze the TiP. When the precursor was completely solidified in the Schlenk, the nanoporous alumina membrane was introduced and kept in contact with the solid surface of the TiP. The Schlenk was then closed and evacuated through the lateral valve (Fig. 2) with the aim of removing all the air from the membrane pores, before being taken out of the liquid nitrogen. The TiP was allowed to melt by reaching room temperature and the membrane sank into the liquid TiP. By opening the valve, the change from vacuum to atmospheric pressure forced the liquid to fill the membrane pores [27]. The template was carefully wiped to remove excess TiP. The subsequent step involved the template being heated in an oven for 15 min at 608 C to decompose the TiP into TiO2. The previously described steps (immersion, freezing, pore filling and decomposition) were repeated with the as- obtained sample to improve the process yield. The sample was finally introduced into a quartz tubular furnace and heated to 500 C for 1 h in air stream to induce the conversion of amorphous TiO2 into its anatase (crystallized) form. After cooling to room temperature, the template was chemically removed in a phosphoric acid (6% wt) and chromic acid (1.5% wt) solution at 80 C for 15 min.

This impregnation–decomposition routine was successively tested with four different TiPs: Titanium isopropoxide (Aldrich), Titanium butoxide (Aldrich), Titanium propoxide (Aldrich) and TiCl4 (Aldrich). In addition, TiPs viscosities were measured by a DV-E viscosimeter (Brookfield Engineering Laboratories) and are listed in Table 1. The nanostructured materials obtained from the different TiPs were characterized by scanning electron microscopy, SEM (Hitachi S-3400N), transmission electron microscopy, TEM (JEOL-200FXII), X-ray diffraction, XRD, (Bruker AXS D8 Advance diffractometer), nitrogen adsorption (Micromeritics ASAP 2020) and Raman spectroscopy (Jovin Yvon HR-8400UV) techniques.

Because of its influence on the pore filling step, vacuum time needed to be optimized in order to control the process yield and consequently maximize TiO2 nanotube production.

Anatase photocatalytic activity measurements

The photocatalytic activity measurements were carried out in a photocatalytic reactor consisting of a 1-L quartz vessel with two valves (air entrance and purge), a sample col-

lector and two UV lamps [Philips TL8W(Hg)]. The lamps emitted a minute fraction of the total radiation at 324 and 325 nm and the rest between 342 and 400 nm with a maximum irradiance peak at 365 nm (3.4 eV). The reactor configuration is schematically represented in Fig. 3. After a check was made that there was no decolourization with UV irradiation or TiO2 alone, 300 mL of 5 ppm MB solution in water was introduced into the reactor together with 100 mg of the tested photocatalyst [the different synthesized TiO2 nanotubes and the commercial anatase (Aldrich, [99%, -325 mesh)]. The mixture was stirred in darkness at 250 rpm for 30 min to assure reactant wall saturation with the MB. The different mixtures obtained were subsequently aerated and illuminated by the UV lamps. 3-mL samples were regularly extracted and filtered. The MB degradation was monitored on a UV–vis Spectrometer (Shimadzu UV-3600) at 662 nm.

Anatase catalyst recycling

After MB photodegradation, the TiO2 catalysts (nanotubes and commercial) were filtered [Omnipore Membrane PTFE (Millipore), 5 μm] and washed with water. They were once again added to the photoreactor to be reused in another MB dye, and photodecompositions were readjusted to keep equivalent experimental conditions in all the cycles.

Results and discussion

During the TiO2 production by the described template method, it was observed that the vacuum time had a significant influence on the material yield. For this reason, it was necessary to optimize this parameter to maximize production of the desired material. Figure 4 plots the evolution of the nanotubes yield production [Yield% = (g TiO2 nanotubes/g template) 9 100] with the vacuum time. A marked increment in the nanotubes yield was registered for the shortest tested vacuum times. A critical vacuum time was found when maximum yield was reached. From this point (critical vacuum time = 60 min for nanotubes obtained from Ti isopropoxide), no increase was observed for longer vacuum times. This critical vacuum time could be interpreted as the moment when the template pores are completely filled.

Figure 5 shows the SEM micrographs corresponding to the TiO2 nanostructures obtained from Ti isopropoxide (a, b), Ti propoxide (c, d), Ti butoxide (e) and TiCl4 (f) following the experimental method described in the previous section. Nanotube structures were

successfully produced from the three first precursors. Only in the case of TiCl4 was the chosen approach not valid because most of the obtained material was amorphous and only a few tube arrays were observed. By examining Fig. 5 in detail, it can be noted that TiO2 nanotubes obtained from Ti isopropoxide (a, b) exhibit longer tubular structures with a lower presence of amorphous material. When nanotubes obtained from Ti isopropoxide (a, b) are compared with those obtained from Ti propoxide (c, d) and Ti butoxide (e), shorter and irregular tube fragments were clearly detected in the two last cases. The morphological differences observed amongst the TiO2 nanotubes obtained from the different TiPs could be related to their different viscosity. In Table 1, the experimental viscosities for the three TiPs are listed. Ti isopropoxide was significantly less viscous than the other TiPs. Thus, Ti isopropoxide would exhibit higher wettability of the alu- mina membranes implying improved accuracy to transfer the tubular morphology of the membrane pores to the resulting TiO2 nanotubes.

TiO2 nanotubes obtained from the isopropoxide pre- cursor were also characterized by TEM. Two representative images are shown in Fig. 6. Tubular hollow structures with a diameter of approximately 200 nm were observed. The final tube diameter is determined by the template pore diameter. The tubes are composed of a single-wrapped monolayer with an estimated thickness of around 20 nm.

BET surface area results for TiO2 nanotubes obtained from the different Ti precursors (excluding TiCl4) are listed in Table 2. Although all the results are comparable, the highest value relates to nanotubes synthesized from the isopropoxide precursor. The role of surface area in the photoactivity efficiency of TiO2 is later discussed in terms of mechanistic considerations.

Figure 7 shows the Raman spectra of the TiO2 nanotubes obtained from the different Ti precursors. TiO2 is known to exist in three crystalline modifications: rutile (tetragonal), anatase (tetragonal) and brookite (ortho- rhombic). Each octahedron in anatase is connected to two edge-sharing octahedrons and eight corner-sharing octahedrons. This occurs in rutile with four edge-sharing octahedrons and four corner-sharing octahedrons [28]. Thus, anatase and rutile have different space groups and, consequently, different vibration active modes. In our case, all registered Raman spectra fitted with that obtained for the commercial anatase. From the group theory analysis, anatase has six Raman active

modes, A1g + 2B1g + 3Eg [28], which are identified at 141 cm-1 (Eg), 195 cm-1 (Eg), 395 cm-1 (B1g), 478 cm-1 (A1g), 514 cm-1 (B1 g) and 638 cm-1 (Eg) with the peak appearing first being the most intense. Nevertheless, two important differences must be considered. The peaks corresponding to the anatase nanotubes appeared broadened and slightly shifted (~11 nm) in comparison with their equivalents in the commercial anatase. The reason for this is that Raman spectroscopy wave vector selection rules, which limit the wave vector of detectable phonons to the Brillouin zone centre, break down at a sufficiently small size [29]. The wall of an anatase nanotube can be understood as a collapse of anatase nanoparticles smaller than those present in commercial anatase powders.

The crystallinity of TiO2 samples can be comparatively evaluated via the relative intensity and resolution of the diffraction peaks of the anatase. Figure 8 shows the XRD patterns of the commercial anatase and the TiO2 nanotubes obtained from the different Ti precursors. The commercial material exhibited higher intensity and narrower peaks than TiO2 nanotubes. TiO2 nanotubes obtained from Ti isopropoxide exhibited slightly higher crystallinity than the nanotubes obtained from the other TiPs.

Anatase is the most popular catalyst for dye contaminant degradation. However, the effect of the structural changes from micro- to nanocrystals must be considered not only in terms of crystal size but also of the induced deformation due to the plane curvature that could affect photocatalyst performance. A few related works can be found in the literature [30, 31], but a detailed study of the photocatalytic properties of TiO2 nanotubes is still required. In this article, the decolourization of MB was monitored as a function of time in the presence of TiO2 anatase nanotubes obtained from Ti isopropoxide, Ti propoxide and Ti butoxide precursors. This dye degradation was also tested in the presence of commercial anatase TiO2 to evaluate the photocatalytic ability of nanotubes in comparison with the commercial photocatalyst.

Figure 9 shows the degradation rate of MB by the anatase TiO2 nanotubes obtained from the three Ti chosen precursors. By comparing nanotubes, the best results in terms of activity were found for those obtained from Ti isopropoxide. This result can be explained as a result of the role played by surface area on the dominant photocatalytic mechanism. There are two proposed mechanisms to explain the dye degradation by anatase [32].

Hole–electron pairs are generated when the anatase is illuminated. In the first mechanism, the dye is attached to the anatase surface. The generated hole migrates to the surface, where electron transfer occurs from the dye molecule to the anatase to neutralize the hole and the dye molecule is consequently oxidized. The second mechanism involves water molecules becoming attached to the anatase surface. In this case, the water molecule is oxidized, and hydroxyl radicals (OH) are generated [$H2O + hole^+ \rightarrow OH + H^+$]. The hydroxyl radical is a very powerful oxidant that is able to migrate to the dye surface and destroy it. By considering that the aromatic groups in MB show great affinity towards the anatase surface, we propose here that the direct dye oxidation attached to the catalyst surface might be the dominant mechanism, which would explain that the nanotubes with the highest surface area exhibit the highest degradation activity [32]. Nevertheless, the experimental results revealed that commercial anatase TiO2 showed a higher degradation rate and, consequently, better photocatalytic activity than all anatase nanotubes, even taking into account the fact that nanotubes have a higher surface area. This can be explained by the higher crystallinity of the commercial anatase [33] observed by XRD. Also, the higher stability of commercial anatase TiO2 powders in water might increase the contact between contaminant and catalyst allowing improved photocatalytic activity. This observation agrees with the literature [31, 34]. Finally, recycling studies were carried out with commercial anatase TiO2 and TiO2 nanotubes obtained from the Ti isopropoxide to compare both materials. The results are shown in Fig. 10. These experiments revealed that TiO2 nanotubes are recovered more efficiently than commercial anatase, with re-utilization of the commercial material being ruled out. The reason for this is that the better stability of commercial anatase microcrystals in water (even forming hydro-colloidal suspensions [34]) limits its recovery by a simple filtration process, which is possible in the case of the anatase nanotubes. After the five consecutive photocatalytic experiments, the recovered materials were characterized by SEM (images not shown), and it was confirmed that the nanotube morphology was not destroyed.

Efficient recovery is an added value for the TiO2 nanotubes catalyst since this allows it to be recycled, in line with the principles of green chemistry. [35].

Conclusions

TiO2 nanotubes were synthesized by a template method based on impregnation–decomposition routines using four different TiPs (Ti isopropoxide, Ti propoxide, Ti butoxide and TiCl4) as channel fillers. It was observed that the vacuum time had a significant influence on the material yield, and a critical value (60 min for Ti isopropoxide experiment) was found corresponding to complete pore filling. The diameter of nanotubes fitted the pore diameter of the anodized alumina membranes used as templates (~200 nm).

TiO2 nanotubes obtained from Ti isopropoxide exhibited the longest hollow tubular structures with lowest presence of amorphous material. The nanotubes synthesized from the isopropoxide precursor also produced the highest surface area values.

Raman and XRD studies of the obtained TiO2 nanotubes confirmed their existence in the anatase crystalline form.

The photoactivity of the anatase nanotubes obtained from Ti isopropoxide, Ti propoxide and Ti butoxide pre- cursors towards MB dye degradation were measured and compared with the commercial anatase photocatalyst. Amongst the synthesized anatase nanotubes, the best results were found for those obtained from Ti isopropoxide. By assuming direct oxidation of the dye molecule attached to the catalyst surface as the dominant mechanism, the experimental observations were consistent with mechanistic considerations; in other words, anatase nanotubes with the highest surface area exhibit the highest degradation activity. Commercial anatase photoactivity towards MB elimination was not improved with regard to degradation rate as its higher stability in water increased the contaminant–catalyst contact. Nevertheless, in comparison with the commercial powders, the more efficient recovery of the synthesized anatase nanotubes, and their consequent recycling supported their utilization as an alternative environmentally friendly photocatalyst in wastewater treatment, in accordance with the principles of green chemistry.

Acknowledgements

Authors sincerely acknowledge J. Sanchez for his helpful contribution to the experimental work. This study was funded by the Government of Aragon and ‘‘La Caixa’’ Ref. GA-LC- 041/2008 and by the Spanish Ministry of Science and Innovation Ref. EUI2008-00152

References

1. Carp O, Huisman CL, Reller A (2004) Prog in Solid State Chem 32:33

2. Zaban A, Ferrere S, Gregg B (1998) J Phys Chem B 102:452

3. O0Regan B, Gra¨tzel M (1991) Nature 353:737

4. Fujishima A, Rao TN, Tryk DA (2000) J Photochem Photobiol C 1:1

5. Kontos AI, Kontos AG, Tsoukleris DS, Vlachos GD, Falaras P (2007) Thin Solid Films 515:7370

6. Choi H, Stathatos F, Dionysiou DD (2006) Thin Solid Films 510:107

7. Mills A, Le Hunte SJ (1997) J Photochem Photobiol A Chem 108:1

8. Rajeshwar K (1995) J Appl Electrochem 25:1067

9. Robinson T, McMullan G, Marchant B, Nigan P (2001) Bioresour Technol 77:247

10. Prado AGS, Torres JD, Faria EA, Dias SCL (2004) J Colloid Interface Sci 277:43

11. Torres JD, Farka EA, Souzade SR, Prado AGS (2006) J Photo- chem Photobiol A 182:202

12. Fujishima A, Hashimoto K, Watanabe T (1999) TiO2 photoca- talysis. Fundamentals and applications. BKC, Tokyo

13. Mardare D, Tasca M, Delibas M, Rusu GL (2000) Appl Surf Sci 156:200

14. Deng ZX, Wang C, Li YD (2002) J Am Ceram Soc 85:2837

15. Lee GW, Choi SM (2008) J Mater Sci 43:715. doi:10.1007/s10853-007-2200-y

16. Tian ZRR, Voight JA, Liu J, McKenzie B, Xu HF (2003) J Am Chem Soc 125:12384

17. Peng TY, Yang HP, Chang G, Dai K, Hirao K (2004) Chem Lett 33:336

18. Miao L, Tanemura S, Kaneko K, Tanemura M (2004) J Cryst Growth 264:246

19. Attar AS, Ghamsari MS, Hajiesmaeilbaigi F, Mirdamadi Sh, 10.1007/s10853-008-2872-y

20. Kasuga T, Hiramatsu M, Hoson A, Sekino T, Niihara K (1999) Adv Mater 11:1307

21. Tsai CC, Teng H (2004) Chem Mater 16:4352

22. Adachi M, Murata Y, Harada M, Yoshikawa S (2000) Chem Lett 29:924

23. Eder D, Kinloch IA, Windle AH (2006) Chem Commun 13:1448

24. Hu MZ, Lai P, Bhuiyan MS, Tsouris C, Gu B, Paranthaman MP, s10853-009-3372-4

25. Ghicov A, Schmuki P (2009) Chem Commun 20:2791

26. Macak JM, Zlamal M, Krysa J, Schmucki P (2007) Small 3:300

27. Michailowski A, Almawawi D, Cheng G, Moskovits M (2001) Chem Phys Lett 349:1
28. Qian L, Du Z-L, Yang S-Y, Jin Z-S (2005) J Mol Struct 749:103
29. Maira AJ, Yeung KL, Lee CY, Yue PL, Chan CK (2000) J Catal 192:185
30. Bavykin DV, Parmon VN, Lapkin AA, Walsh FC (2004) J Mater Chem 14:3370
31. Yu YX, Xu DS (2007) Appl Catal B 73:166
32. Ishibashi K, Fujishima A, Watanabe T, Hashimoto K (2000) J Photochem Photobiol A 134:139
33. Yu J, Wang G, Cheng B, Zhou M (2007) Appl Catal B 69:171
34. Prado AGS, Costa LL (2009) J Hazard Mater 169:297
35. Prado AGS (2003) Quim Nova 26:738

Figures

Tables

Figure 1

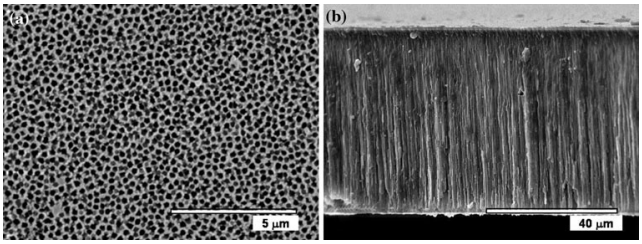

Figure 2

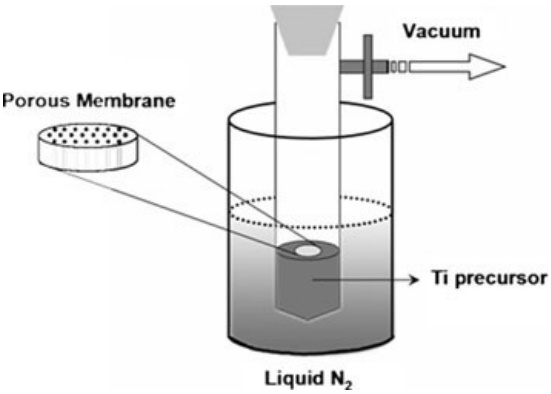

Figure 3

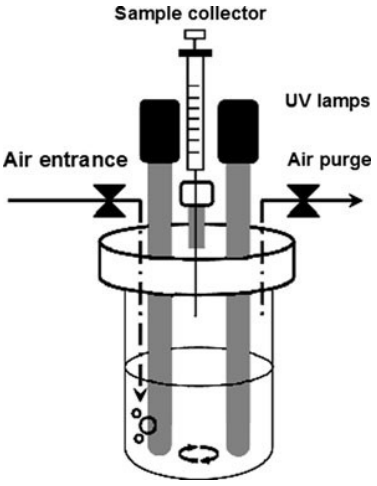

Figure 4

Figure 5

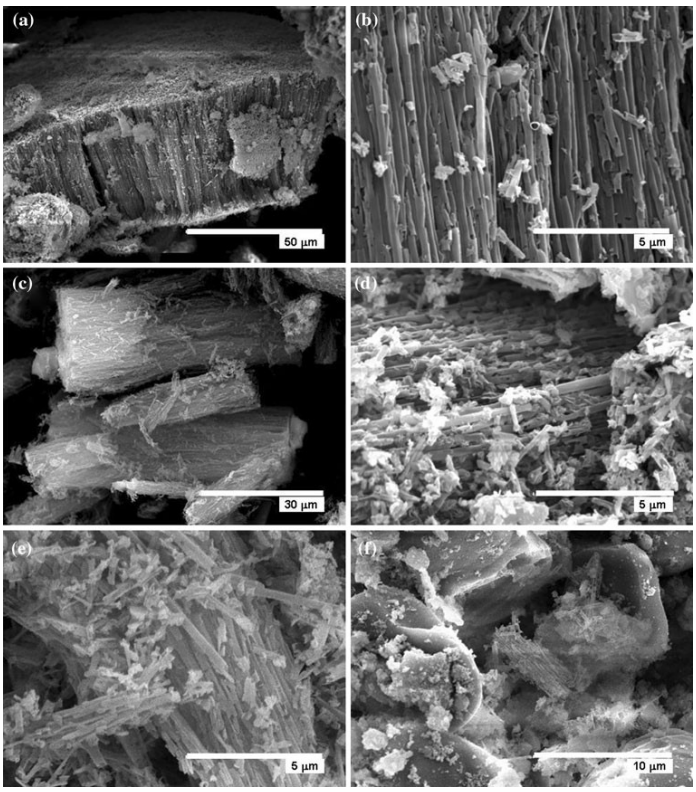

Figure 6

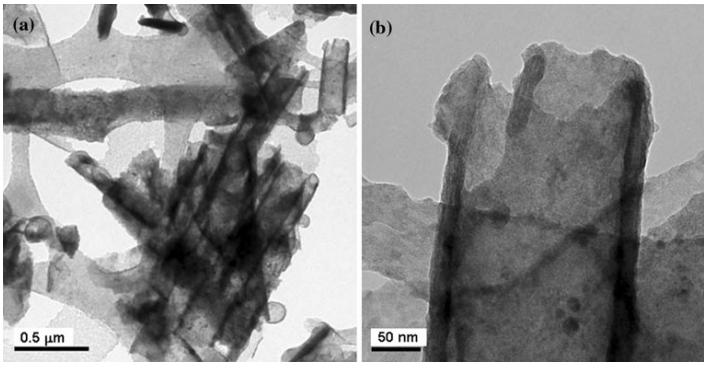

Figure 7

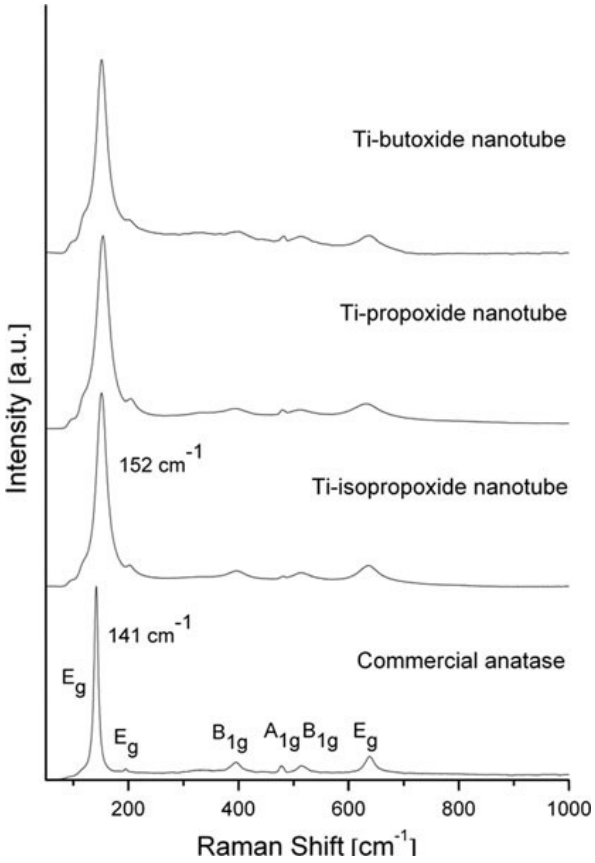

Figure 8

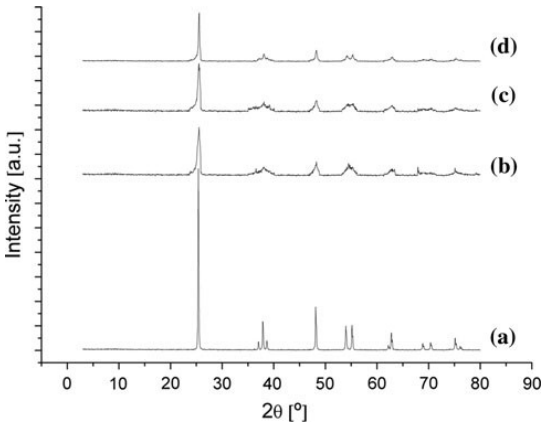

Figure 9

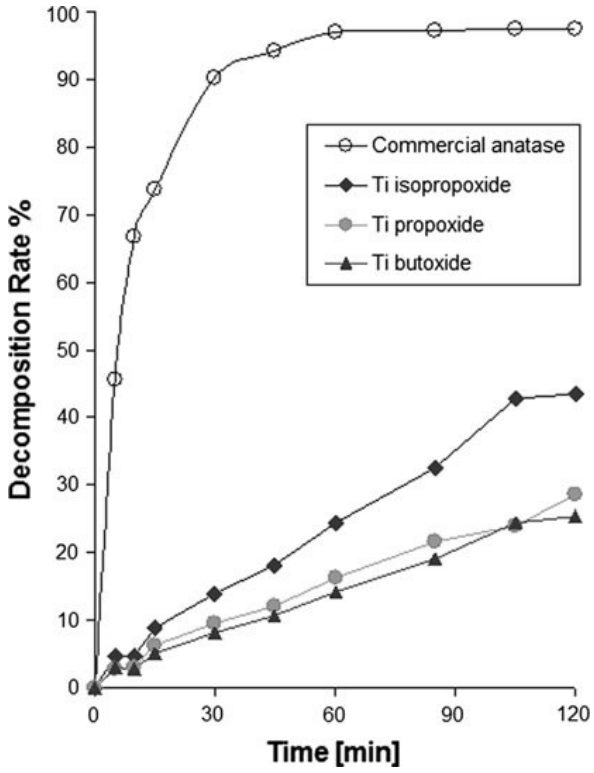

Figure 10

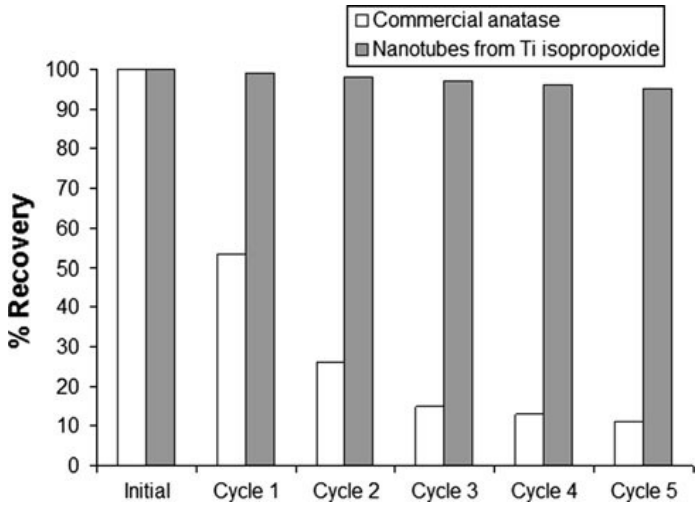

Table 1

Ti precursor	Viscosity (cP) at 25 °C
Ti isopropoxide	71.85
Ti propoxide	348.28
Ti butoxide	1136.26

Table 2

Tio_2 material	BET surface (m^2/g)
Commercial anatase	8
Ti isopropoxide-nanotubes	54
Ti propoxide-nanotubes	36
Ti butoxide-nanotubes	32